# Matrix cracking initiated by fibre breaks in model composites

A. N. GENT, C. WANG
*Institute of Polymer Engineering, The University of Akron, Akron, OH 44325, USA*

Fracture of resin in a composite material can be initiated by a tensile break in a fibre. This process has been investigated for a simple model composite, consisting of two inextensible rods placed along the axis of a cylindrical elastic block and touching in the centre. The rods represent a broken fibre. Energy release rates, *G*, were calculated by finite element methods for a circular crack growing outwards from the point where the rod ends separated as they were pulled apart. Results are compared with experimental observations on cracking of a silicone rubber cylinder containing two steel rods. It was found that a crack grew outwards under increasing load until its radius reached a certain size, approximately half-way to the surface of the resin cylinder. At this point, *G* reached a minimum value and then increased. Simultaneously, the crack accelerated and the sample broke. Forces required to propagate the crack were successfully predicted by linear elastic fracture mechanics at all stages of crack growth and for a wide range of fibre and sample radii. In particular, good agreement was obtained with the maximum force that the model system could support, i.e. the breaking load. When the sample was surrounded by a rigid tube, representing neighbouring fibres surrounding the broken one, growth of a crack required an increasing load at all stages. The sample finally fractured when the broken fibre pulled out with resin still attached to it. Application of these results to unidirectional fibre-reinforced materials is discussed.

## 1. Introduction

Fibre-reinforced composites are lightweight and strong materials, with several possible modes of rupture. At present there is no satisfactory theory relating strength of composites to properties of the constituent materials, even in the simplest cases. Two models of a composite with continuous fibre reinforcement are employed here to study the consequences of a fibre break. The first model is shown in Fig. 1a. Two identical steel rods were embedded along the axis of a cylindrical block of silicone rubber resin, with their ends in contact. They were treated with a primer to give good bonding to the silicone rubber. Because of the great difference in Young's modulus of steel and silicone resin, the rods can be considered to be inextensible in comparison with the elastic matrix. Thus, when the sample is put under a tensile load all of the strain energy is stored in the matrix resin, assumed for simplicity to be linearly elastic.

The second model was used to investigate the effect of neighbouring fibres on a crack propagating outwards from the initial break. This is shown in Fig. 1b. It differs from the first model by the addition of a rigid tube enclosing the resin cylinder and bonded to it. The sample thus consists of a tube of silicone resin, bonded to a broken rigid fibre at its centre, and to a concentric rigid tube surrounding it. The external tube represents the ring of parallel fibres surrounding a given fibre in a multi-fibre composite. Strong bonding between the

resin, the central fibre, and the external tube, ensured that adhesive failures did not occur in the experiments.

A Griffith fracture criterion is applied, as follows [1]:

$$-\partial W/\partial A|_l \geq G_c \qquad (1)$$

where *W* is elastic strain energy stored in the system (in the present case, in the resin only), *A* is crack area and $G_c$ is fracture energy of the resin. The derivative is evaluated at constant length, *l*, and hence displacement, so that the applied force does no further work as the crack grows. Thus, energy required for fracture is obtained solely from elastically stored energy. The left-hand side of Equation 1, termed the strain energy release rate, is denoted *G* hereafter.

Equation 1 gives a necessary condition for a crack to propagate: the rate of release of strain energy must reach a critical value. In some cases, crack growth will be stable, i.e. the applied load must be increased to grow the crack further. In other cases growth is unstable, resulting in catastrophic failure. The criterion for stable growth is

$$dG/dA \leq 0 \qquad G = G_c \qquad (2)$$

When a fibre breaks, two types of failure may ensue. A debond may propagate along the fibre/matrix interface in the form of a cylindrical crack running in the fibre direction, or a planar (circular) crack may grow outwards into the matrix material at right angles to the fibre. Which mode of failure takes place depends
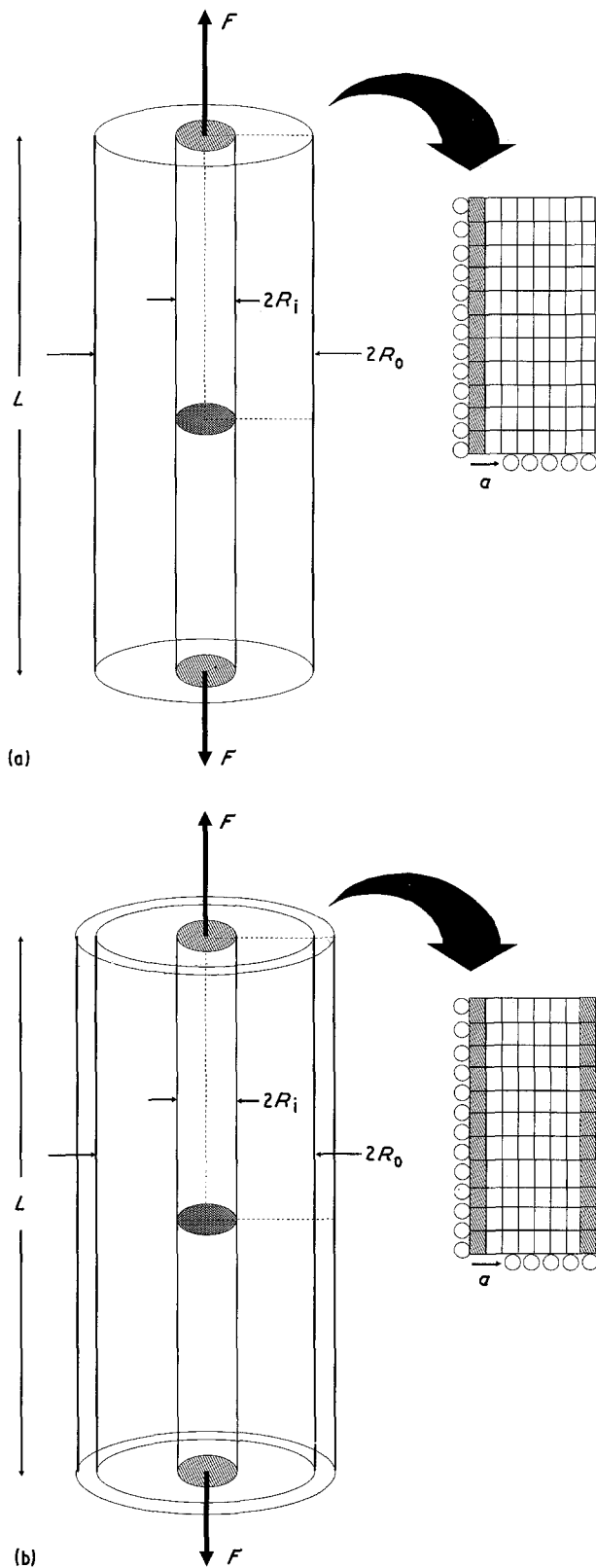
*Figure 1* (a) Sketch of the first model. A resin block contains two rods with their ends touching, representing a broken fibre. (b) Sketch of the second model. A rigid tube, representing unbroken fibres, surrounds a resin cylinder containing a broken fibre.

on the geometry and mode of loading of the specimen and the relative strength of adhesion compared to strength of the resin. If adhesion is relatively weak, a crack will propagate along the interface as a debond. On the other hand, if adhesion is strong, then a perpendicular crack will grow outwards into the resin – which is the case considered here.

Debonding of fibres, "pull-out", and repeated fracture of fibres as a result of progressive failure of the bond between fibre and resin, have been examined elsewhere [2–5]. A critical force is required to initiate an interfacial crack at the fibre end. Values were calculated from a Griffith fracture criterion, Equation 1, with $G_c$ replaced by a fracture energy for rupture of the interfacial bond, denoted $G_a$ [6]. (Values of $G_a$ are generally smaller than $G_c$.)

As a fibre is debonded, frictional resistance to pull-out increases and the force needed to propagate the debond increases continuously with the length debonded [3]. This effect can lead to repeated breaking of the fibre, termed "fragmentation". The frictional effect has been minimized in other work by using "push-out", instead of "pull-out", mechanics [4]. In practice, the main parameter which determines whether debonding will occur or not in a given composite, is $G_a$, the energy required to debond unit area of the fibre–matrix interface.

Compared with fibre pull-out, the mechanics of resin cracking have received little attention. Results for two extreme cases are well-known. Growth of a small penny-shaped crack of radius $a$ in a homogeneous material has been analysed by Sack [7]. The critical far-field tension stress is

$$\sigma^2 = \pi E G_c / 3a \qquad (3)$$

The corresponding problem for a circular debond located at the interface between an elastic half-space and a rigid substrate was solved by Mossakovskii and Rybka [8]. The result is similar

$$\sigma^2 = 2\pi E G_c / 3a \qquad (4)$$

the additional factor of 2 arising from the presence of elastically stored energy in only one-half of the composite.

These examples can be regarded as extreme cases of matrix cracking [2]. They both predict catastrophic growth of the initial crack when the critical condition is achieved, because the stress required to propagate a crack decreases as the crack radius increases. The more complex case when a broken fibre is the initiator of a crack has been considered by Mullin *et al.* [9]. They considered a single inextensible fibre embedded in an elasto-plastic resin and found that either one circular crack, two inclined-conical cracks, both, or neither, formed at the break and grew into the matrix. Which process occurred depended on the particular combination of fibre and matrix considered. Mahishi and Adams [10, 11] used a finite element model (FEM) to examine crack propagation in an elasto-plastic matrix material. They found that the stress intensity factor increased with crack radius up to a certain point. Thereafter, unstable crack growth was predicted to occur.

A greater release of strain energy may be obtained for a cylindrical crack that propagates along the fibre, in the resin but as close to the fibre as possible, rather than for a circular crack growing at right angles to the fibre. This is probably the case when the fibre radius is small in comparison to the radius of the cylinder of resin [2]. We are concerned here only with growth of

circular cracks, as observed when the fibre radius is relatively large compared to that of the resin cylinder surrounding it and the bonding between fibre and resin is strong.

Experimental measurements of crack growth and breaking force have been carried out for the simple two-rod model, using various ratios of rod radius to resin cylinder radius. The results are compared with theoretical predictions from FEM calculations. The objectives of the study are to elucidate the principal factors affecting resin cracking initiated by a broken fibre and to predict the strength of a model fibre composite when this is the mode of failure. The analysis is also relevant to the widely used "fragmentation test" for adhesion between resin and fibre [12–15].

## 2. Stress intensity factors and strain energy release rate

The stress field around a broken fibre end is quite complex and analytical solutions are rather difficult to obtain. Finite element numerical techniques have been widely used, therefore, to determine crack tip stress fields and stress intensity factors. In some cases special crack tip elements were employed to deal with the stress singularity at the crack tip [16]. But stress intensity factors can also be derived from energy release rates, as described below. Finite element methods were used here to derive values of energy release rate, $G$, for various sizes of crack in the resin, from the effect of a crack on the sample compliance. Dixon [17] showed that the stress field in the immediate vicinity of the crack tip makes relatively little contribution to the overall displacement of the system, and hence to the compliance, so that excessive refinement of the mesh at the crack tip is not necessary. This is the principal advantage of energy methods as employed here.

The first step is to calculate the elastic compliance, $C$, of specimens containing cracks of increasing radius, $a$. Strain energy release rates associated with the creation of a new crack surface are then obtained by numerical differentiation of the relation between compliance and crack area, $A$ [18]

$$G = (F^2/2)\partial C/\partial A = (F^2/4\pi a)\partial C/\partial a \qquad (5)$$

The following procedure was employed. First, for a given value of crack radius, $a$, the displacement, $\delta$, was calculated for a given tensile force, $F$, applied to the outer ends of the rods. In this way the compliance, $C$, was determined, $C = \delta/F$. Then, by incrementing the crack radius, the rate of change of compliance with crack radius was evaluated and hence $G$ found from Equation 5. Finally values of the applied force, $F$, at which a given crack would grow were calculated from Equation 5 by replacing the value of $G$ with its critical value, the fracture energy, $G_c$, of the resin. Hence

$$F^2 = 4\pi a G_c/(\partial C/\partial a) \qquad (6)$$

In linear elastic fracture mechanics, the relation between energy release rate and stress intensity factor, $K$, in plane strain is [18]

$$K^2 = EG/(1 - v^2) \qquad (7)$$

where $E$ is Young's modulus and $v$ is Poisson's ratio of the resin. The dimensionless stress intensity factor, $Y$, is defined by [18]

$$K = Y\sigma (\pi a)^{1/2} \qquad (8)$$

where $\sigma$ is the far-field stress $= F/\pi R_o^2$, where $R_o$ is the radius of the resin block. Values of $K$ and $Y$ can thus be calculated from $G$ by means of Equations 7 and 8, and values of breaking force, $F_b$, obtained on substituting a critical value for $K$, denoted $K_c$, in Equation 8. Thus, exactly equivalent calculations can be carried out in terms of stress intensity, $K$, and its critical value, $K_c$, in place of strain energy release rate, $G$, with a critical value, $G_c$.

## 3. Experimental procedure and FEM calculations

### 3.1. Preparation of test pieces and properties of the resin

Transparent silicone resin (Sylgard S-184, Dow Corning Corporation) containing 10% by weight of curing agent (Sylgard C-184, Dow Corning Corporation) was used as matrix material, and flat-ended steel rods as fibres. To obtain good bonding to the resin the cylindrical surfaces of the rods were first polished with fine emery paper, cleaned with isopropanol and dried. They were then immersed in Primer 92-023 (Dow Corning Corporation) for 24 h. A small amount of partially cured resin was used to glue two rods together end-to-end. The joined rods were then carefully placed along the axis of a plastic tube, used as a mould for casting the cylinder of resin. Uncured silicone resin was poured into the tube to surround and encapsulate the steel rods. Curing was effected by heating the assembly for 12 h at 110 °C. Samples were made with different combinations of rod radius, $R_i$, and external radius, $R_o$, of the resin cylinder: $R_i = 0.435$–$1.16$ mm; $R_o = 3.0$ and $5.6$ mm. All samples had a length, $L$, of 50 mm.

For the second set of experiments, glass tubes were bonded to the external surface of the cured resin cylinder to simulate the constraints due to neighbouring fibres. The internal and external radii of the glass tubes were 3 and 4 mm, respectively. Strong bonding between the silicone resin and glass was obtained by immersing the tubes in a 50% solution of adhesive primer in heptane for 12 h and then drying them at room temperature before use. Rods, glued together, were placed along the axis of the tube, which was then filled with uncured resin. Curing was effected at room temperature for 7 days to avoid cracking caused by shrinkage stresses, either at the fibre/resin or tube/resin interface, that was encountered on cooling from an elevated curing temperature. Typical dimensions of a specimen were: rod radius $R_i = 0.435$ mm, external radius, $R_o$, of the resin cylinder equal to 3.0 mm, overall length, $L$, of cylinder equal to 50 mm.

Tensile stress–strain relations for the cured silicone resins were found to be quite linear up to about 30% strain. Young's modulus, $E$, was determined from the slope at small strains to be 2.8 MPa for samples cured at 110 °C and 0.87 MPa for samples cured at room temperature.

Fracture energies, $G_c$, of silicone resin were determined at different rates of tear propagation, from measurements of the average force required to propagate a tear. The results are plotted in Fig. 2 against the rate of tearing. Results for both curing conditions were approximately the same, even though the values of tensile modulus were quite different. As for other viscoelastic materials, there is a considerable effect of tear rate, the value of $G_c$ increasing from about $180 \, \text{J m}^{-2}$ at a rate of $0.8 \, \mu\text{m s}^{-1}$ to about $330 \, \text{J m}^{-2}$ at a rate of $2 \, \text{mm s}^{-1}$. In experiments with both models of a composite, crack growth took place at rates lying in the relatively narrow range: $5$–$25 \, \mu\text{m s}^{-1}$. Thus, the relevant value of $G_c$ in the fracture experiments was $200$–$230 \, \text{J m}^{-2}$.

Figure 3 Force–displacement relation for a sample with a propagating crack. $R_i = 0.435 \, \text{mm}$, $R_o = 3.0 \, \text{mm}$.

## 3.2. Measurement of crack size and sample compliance

Specimens were loaded in tension using an Instron tensile testing machine equipped with a microscope, video camera and recorder to study crack growth as the applied tensile load was increased continuously. When the steel rods were pulled apart, a crack initiated at the point where they were initially in contact, and grew transversely across the matrix. Its radius, $a$, was measured as the distance from the axis of the rods to the crack tip. The relation between load and displacement was recorded simultaneously, and the compliance of a specimen containing a crack of a given radius was derived from the chord of the displacement–load relation at the appropriate displacement, as shown in Fig. 3. Compliances for various crack radii were obtained in this way in a single experiment. A relatively slow rate of stretching, of $8 \, \mu\text{m s}^{-1}$, was employed. All measurements were carried out at room temperature, about $23 \, ^\circ\text{C}$.

Owing to its cylindrical surface, the transparent silicone resin served as a lens and magnified the size of the crack. The degree of magnification was approximately constant as the crack grew, given by the refractive index of the resin, $1.41$ (see Appendix 1). Corrections were made to the observed crack radius to allow for this magnification.

In contrast, the applied tensile stress, enhanced somewhat by stress concentrations near the crack tip, caused the resin cylinder to undergo Poissonian con-
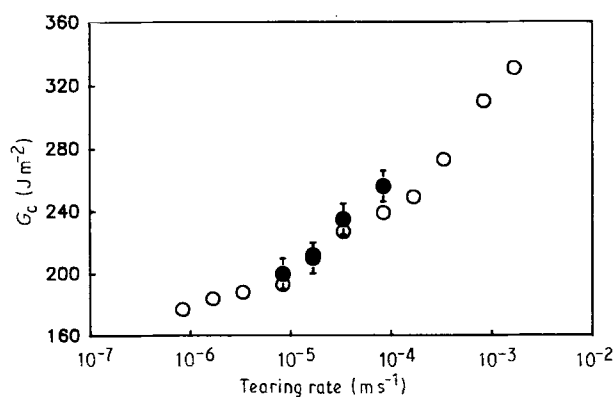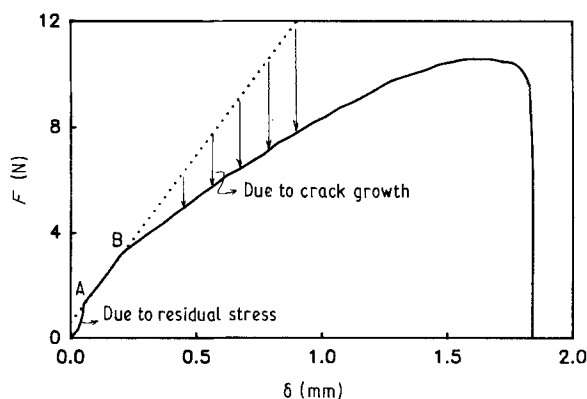
traction and the crack became smaller in radius than in the unstressed state. A correction for the amount of contraction was deduced by FEM, as described in Appendix 2. Generally speaking, the effect of magnification on the apparent crack size was about $+ 40\%$, and that of Poissonian contraction was about $- 10\%$.

Fig. 3 shows a typical force–displacement relation for a model composite specimen without external constraints, loaded in tension. It is linear initially, up to the point B. Non-linearity starting at B is attributed to crack propagation. Thus, the load at B, about $3.0 \, \text{N}$, is taken as the force required to initiate growth of a crack with a radius given by the rod radius. Then, as the crack grew, the compliance of the specimen increased continuously.

Linear elastic behaviour of a cracked specimen was verified by stretching a sample with a large-diameter crack already developed at the rod end, and then unloading the specimen before the crack started to grow further. A linear relation was obtained between load and displacement for this cracked specimen, with virtually no hysteresis between loading and unloading relations.

## 3.3. Pre-stress due to thermal contraction

A curious feature of the experimentally determined relations between load and displacement was a small offset in the initial portion of the force–displacement curve (region O–A in Fig. 3). In effect, a certain force was required to pull the rods apart initially. This is attributed to a prestress set up by differential thermal contraction between the rods and resin as the specimen was cooled down from curing temperature to room temperature. As a result, a shrinkage stress developed in the resin, pulling the rods together. The shrinkage force could be estimated by extrapolating the linear behaviour observed at small displacements (region A–B) back to the load axis. A residual force of about $0.9 \, \text{N}$ was deduced in this way, approximately $8\%$ of the maximum load required to break the sample. Fig. 4 shows the variation of residual force with test temperature. It decreased continuously, becoming zero at $100 \, ^\circ\text{C}$, close to the curing temperature, confirming that the source of this anomalous

Figure 2 Fracture energy, $G_c$ versus tearing rate for silicone rubber samples cured at ($\bigcirc$) $110 \, ^\circ\text{C}$ and ($\bullet$) room temperature.
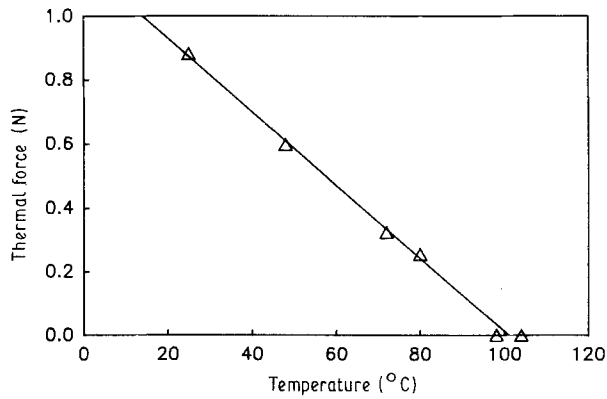
*Figure 4* Variation of residual compressive force with temperature. $R_i = 0.435$ mm, $R_o = 3.0$ mm.

feature of the load–displacement relation at room temperature was a compressive pre-load caused by thermal shrinkage of the resin. In contrast, there was no thermal contraction in the second composite model because the resin was cured at room temperature in that case.

## 3.4. Numerical calculations

An ADINA FEM program [20] was used to calculate compliances of a specimen with different crack radii. Eight-noded quadrilateral axisymmetric elements with four integration points were used. The mesh is shown in Fig. 5. Because of the symmetry of the system, only one-half of the specimen was modelled. In the radial direction 15 elements were employed, and 30 elements in the axial direction, between the rod end and upper end of the cylinder. For the second model, with external constraints imposed by the outer rigid tube, all nodes on the outer surface, radius $R_o$, were fixed. The maximum aspect ratio of mesh elements was about 10.

Both rods and resin were assumed to be linearly elastic and nearly incompressible, with Poisson's ratio of 0.4999. To make the rods effectively rigid, Young's modulus was made $10^9$ times that of resin. Perfect bonding was assumed to exist between the rods and resin (and between the resin and external tube, in the second model). Different radii $R_i$ and $R_o$ were employed, with the ratio $R_i/R_o$ ranging from 0.053–0.8. The ratio of cylinder length, $L$, to resin radius, $R_o$, was chosen to be large enough to minimize end effects and still give adequate accuracy for determining small changes in compliance with crack radius. Preliminary results indicated that a value of 16.6 was satisfactory in this respect; it was used in all the cases reported here. Most of the calculations were carried out for a representative specimen with dimensions: $R_i = 0.435$ mm, $R_o = 3$ mm, $L = 50$ mm.

## 3.5. Test of validity of FEM results

The validity of the FEM model was examined by solving a simple case for which an analytical solution is already known. A penny-shaped crack in the centre of a homogeneous elastic cylinder under tension has
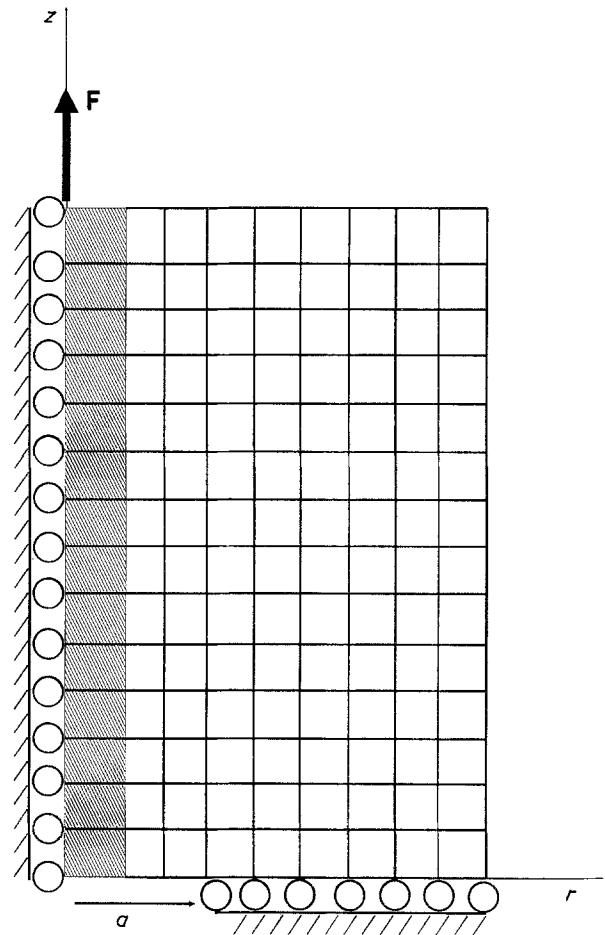


*Figure 5* Sketch of finite element grid for a sample containing a crack of radius, $a$. The shaded area represents the embedded rod (fibre).

been widely investigated [21]. An approximate solution for a dimensionless stress intensity factor, denoted $Y'$ and defined by the relation

$$K = \pi^{1/2} Y' a^{1/2} [1 - (a/R)]^{1/2} [F/\pi(R^2 - a^2)] \quad (9)$$

was obtained by cubic interpolation [21]. This takes the form

$$Y' = (2/\pi) [1 + (1/2)(a/R) - (5/8)(a/R)^2] + 0.268 (a/R)^3 \quad (10)$$

When the crack size is much smaller than the radius, $R$, of the cylinder, the value of $Y'$ (now equal to $Y$, Equation 8) is $2/\pi$, in agreement with Sack's result, Equation 3.

Values of the compliance, $C$, and its derivative, $\partial C/\partial A$, with crack area were calculated using the present finite element model. Values of $Y'$ calculated from them by means of Equations 5, 7 and 9 are compared with values from Equation 10 in Fig. 6. Agreement is quite good, within 5% over most of the range of crack radius. Discrepancies for extremely small and extremely large cracks are attributed to the use of only 15 elements to represent the entire radial distance for crack growth. Thus, small cracks were represented by only one or two elements and, for large cracks, only one or two elements remained unbroken. FEM results would not be expected to be highly accurate under these circumstances.
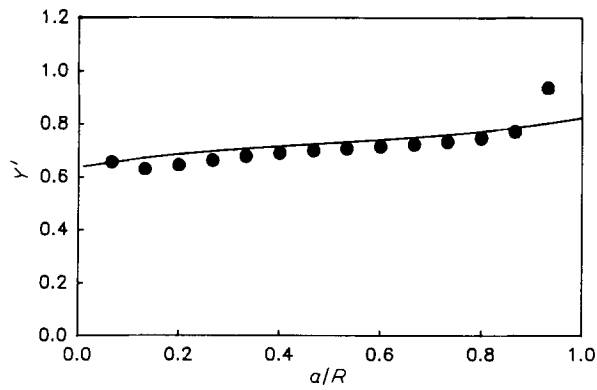
Figure 6 Comparison of (●) FEM results for stress intensity factor, $Y'$, (defined by Equation 9) for a penny-shaped crack in a solid cylinder, with (——) values calculated from Equation 10. Dimensions of cylinder: radius = 3.0 mm, length = 50 mm.

## 4. Results and discussion

### 4.1. Results for an unrestrained sample (Model 1)

#### 4.1.1. Compliance as a function of crack size

Values of compliance were calculated as a function of crack radius for various values of rod radius, $R_i$, and sample radius, $R_o$. Results for specimens with an external radius, $R_o$, of 3 mm are plotted in Fig. 7. The compliance increased with increasing crack size, in an approximately linear way, and then more rapidly as the dimensionless crack radius $(a - R_i)/(R_o - R_i)$ exceeded about 0.6. And the larger the radius of the enclosed rods, the lower was the compliance. Similar relations were obtained for samples with different external radius, $R_o$. As expected, the compliance was smaller for samples of larger radius.

In the experiments, a circular crack was found to grow symmetrically, under increasing load, until it reached a certain size, about half-way to the edge of the sample. The load then decreased slightly and catastrophic failure followed immediately. Stages in the growth of a typical crack are shown in Fig. 8. Values of sample compliance were recorded continuously as the crack grew, until the sample fractured. Fig. 9 shows a comparison of compliance results from FEM and from direct measurement. Good agreement is seen to hold where comparison is possible, i.e. until catastrophic failure intervened.
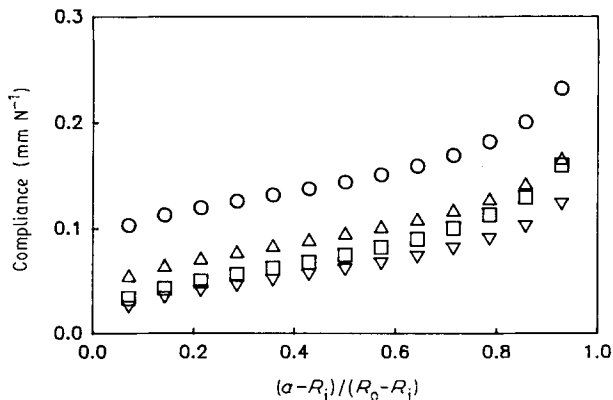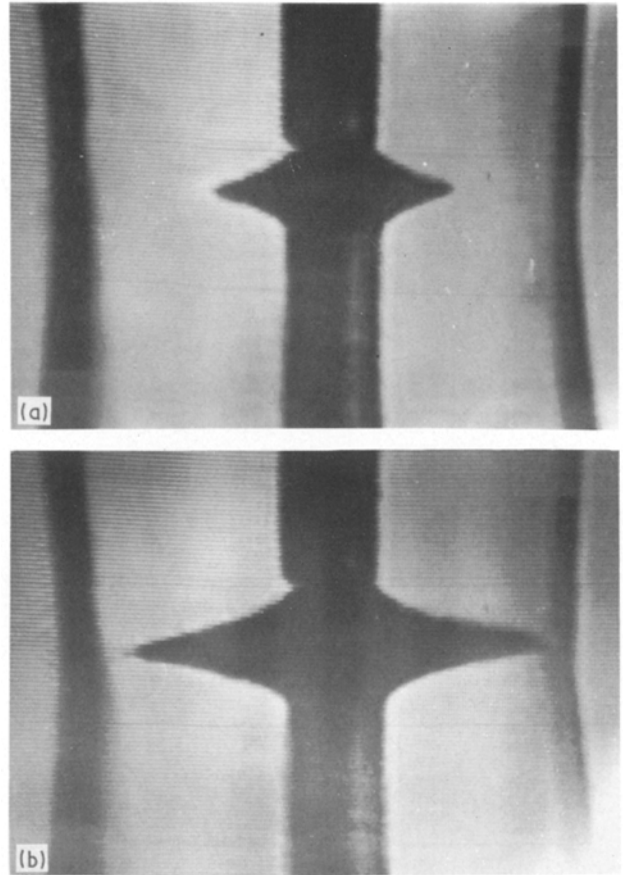


Figure 8 (a, b) Cracks photographed at different stages for a sample with rod radius $R_i = 0.435$ mm, external radius $R_o = 3.0$ mm.
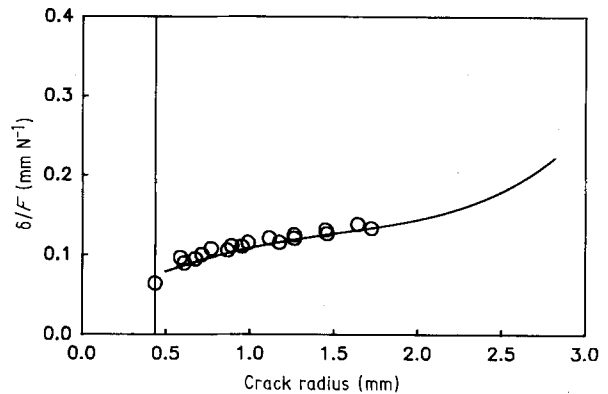


Figure 9 Comparison of (○) measured and (——) calculated compliances as a function of crack radius, for a sample of 3.0 mm external radius. The vertical line denotes the rod radius, $R_i$.

### 4.1.2. Energy release rates and breaking forces

Rates of change of compliance with crack area $\partial C/\partial A$ were calculated by a central difference method using three successive values of $C$ as a function of crack radius. From these results, values of $G$ for a unit applied tensile load were obtained using Equation 5. They are plotted in Fig. 10 as a function of dimensionless crack radius, for samples with an external radius of 3 mm and different rod radii. Initially, $G$ decreases with increasing crack size and then passes through a broad shallow minimum at a dimensionless crack radius of about 0.5. Similar results were obtained for different rod radii and with other sample radii.
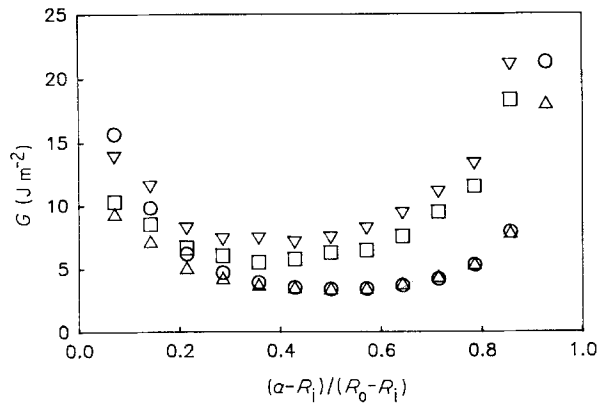


Figure 7 Calculated compliances of Model 1 specimens versus dimensionless crack radius $(a - R_i)/(R_o - R_i)$. $R_i$ (mm): (○) 0.3, (△) 1.0, (□) 2.0, (▽) 2.4; $R_o = 3.0$ mm.

*Figure 10* Calculated energy release rate, $G$, for unit applied load versus dimensionless crack radius $(a - R_i)/(R_o - R_i)$. $R_i$ (mm): (○) 0.3, (△) 1.0, (□) 2.0, (▽) 2.4, $R_o = 3.0$ mm.
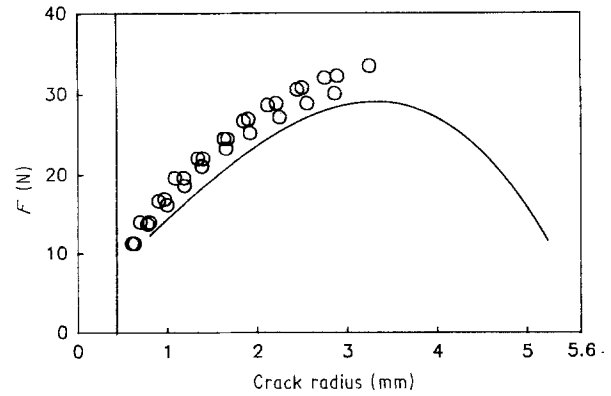


*Figure 12* Comparison of applied load $F$ versus crack radius, (——) calculated by FEM, with (○) experimentally measured values. The vertical line denotes the rod radius, $R_i$.

Corresponding values of force, $F$, required to propagate a crack were then calculated from Equation 6, using the appropriate value of fracture energy, $G_c$, of 230 J m$^{-2}$ for the silicone resin used in the experiments. They are represented in Fig. 11 by a continuous curve. As a crack starts to grow from its initial size, given by the rod radius, an increasing load is seen to be needed to propagate it. Thus, crack growth is initially stable. But after the required force passes through a maximum (and the energy release rate passes through a minimum), the system becomes unstable and catastrophic failure ensues.

Experimental measurements of crack radius are plotted in Figs 11 and 12 against the applied load, for comparison with calculated values. Good agreement was obtained, both in the general form of the relation for crack propagation force as a function of crack radius, and in the breaking force when the crack reaches a critical size. A similar degree of agreement was obtained with rods and samples of various radii. Thus, the theoretical treatment appears to describe the process of crack growth with considerable success. Experiments could not be continued beyond a dimensionless crack radius of about 0.5 because the samples broke at this point, as predicted.

### 4.1.3. Stress to initiate crack growth

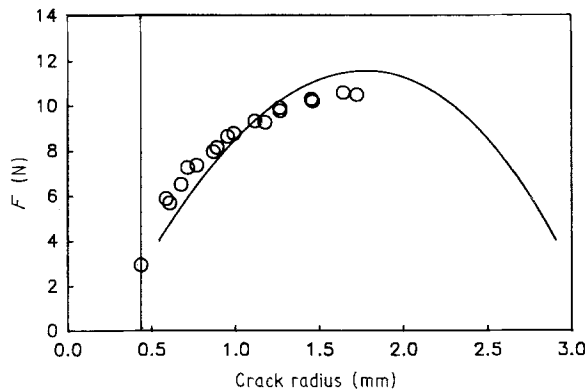The applied force, $F_i$, and corresponding stress, $\sigma_i$,



*Figure 11* Comparison of applied load $F$ versus crack radius, (——) calculated by FEM, with (○) experimentally measured values. The vertical line denotes the rod radius $R_i$.

required to initiate crack growth were estimated using Equation 6. Initial values of $G$ were obtained by fitting calculated values to a five-term polynomial function of crack radius and then extrapolating back to a crack radius equal to that of the rod. Values of $F_i$ and $\sigma_i$ obtained in this way are given in Table I. They increase as the radius of the rods, and hence the radius of the starter crack, increases. This is in striking contrast to an isolated circular crack, Equation 3, where larger cracks require smaller stresses to propagate them. Apparently the presence of rigid bonded rods has a protective effect on cracks formed at their ends.

The effect of sample radius is also shown in Table I. For a given rod radius, the stress, $\sigma_i$, required to initiate a crack was found to decrease as the sample radius increased, although the force, of course, increased.

### 4.1.4. Breaking stress

Values of breaking force, $F_b$, and breaking stress, $\sigma_b$, were calculated from minimum values of $G$, using Equation 6. The results are given in Table I. When the rod radius was smaller than about $0.5R_o$, the minimum value of $G$ was found to be approximately constant, and was reached at a critical crack radius, $a_c$, of about $(R_i + R_o)/2$, i.e. when the crack was about half-way to the edge of the sample. On the other hand, when the rod radius was larger than about $0.5R_o$, the minimum value of $G$ was larger and occurred at a smaller crack radius. In other words, when the rod radius is smaller than about one-half of the sample radius, fracture would be expected at a dimensionless crack radius of about 0.5 at a constant force, independent of rod radius, but when the rod radius is larger than this, fracture is predicted to occur at an earlier stage of crack growth and at a smaller force. In contrast, the force required to start a crack growing depends directly upon its initial radius, $R_i$, as shown in Table I: the larger the value of $R_i$, the larger the force needed to initiate crack growth. Experimental results were in good agreement with these predictions in all cases.

Samples with a larger external radius were found to break at a lower stress, even though the breaking force

TABLE I Calculated and measured forces, $F$, and stresses, $\sigma$, to initiate a crack ($F_i$, $\sigma_i$) and cause catastrophic rupture ($F_b$, $\sigma_b$) in Model 1 specimens

| $R_i$ (mm) | $R_o$ (mm) | Calculated | | | | Measured | | Calculated | |
| --- | --- | --- | --- | --- | --- | --- | --- | --- | --- |
| | | $F_i$ (N) | $\sigma_i$ (N mm$^{-2}$) | $F_b$ (N) | $\sigma_b$ (N mm$^{-2}$) | $F_i$ (N) | $F_b$ (N) | $a_c^a$ (mm) | $\sigma_b^b$ (N mm$^{-2}$) |
| 0.16 | 3.0 | 2.5 | 0.09 | 11.9 | 0.42 | | | 1.58 | 0.65 |
| 0.3 | 3.0 | 3.0 | 0.11 | 11.7 | 0.41 | | | 1.65 | 0.64 |
| 0.435 | 3.0 | 3.5 | 0.12 | 11.3 | 0.40 | 2.9 | 10.6 | 1.72 | 0.63 |
| 0.6 | 3.0 | 4.0 | 0.14 | 11.1 | 0.39 | | | 1.80 | 0.61 |
| 0.78 | 3.0 | 4.6 | 0.16 | 12.0 | 0.42 | 3.9 | 10.9 | 1.89 | 0.60 |
| 1.0 | 3.0 | 5.1 | 0.18 | 11.6 | 0.41 | 4.7 | 11.2 | 2.00 | 0.58 |
| 1.16 | 3.0 | 5.2 | 0.18 | 11.5 | 0.41 | 5.5 | 10.6 | 2.08 | 0.57 |
| 1.5 | 3.0 | 5.5 | 0.19 | 10.7 | 0.38 | | | 2.25 | 0.55 |
| 2.0 | 3.0 | 5.1 | 0.18 | 9.1 | 0.32 | | | 2.42 | 0.53 |
| 2.4 | 3.0 | 4.2 | 0.15 | 8.1 | 0.29 | | | 2.64 | 0.51 |
| 0.435 | 0.545 | 0.4 | 0.43 | 0.6 | 0.62 | | | 0.49 | 1.17 |
| 0.435 | 1.45 | 1.3 | 0.20 | 3.7 | 0.56 | | | 0.94 | 0.85 |
| 0.435 | 2.18 | 2.2 | 0.15 | 6.8 | 0.46 | | | 1.31 | 0.72 |
| 0.435 | 5.6 | 6.9 | 0.07 | 28.6 | 0.29 | 11.3 | 32.3 | 3.02 | 0.47 |

$^a$ Value when $G$ is a minimum.
$^b$ Calculated from Equation 3 at the critical crack radius, $a_c$.

was higher, Table I. In fact, the breaking stress was somewhat smaller (0.55–0.7 times) than the corresponding value for an isolated circular crack of the same radius in a homogeneous solid, Table I. Thus, although embedded rods strengthen a sample initially and prevent small cracks from growing catastrophically, they have a slight weakening effect when the crack reaches its critical size.

It should be noted that the stress to fracture a composite depends on both $R_i$ and $R_o$ separately, and not on the ratio $R_i/R_o$. For example, if we compare a sample with $R_i = 2.4$ mm and $R_o = 3.0$ mm with another sample with $R_i = 0.435$ mm and $R_o = 0.545$ mm, both composites have the same $R_i/R_o$ ratio but the breaking stresses are different: 0.29 and 0.62 N mm$^{-2}$.

All of the FEM results indicate the rather surprising feature that a crack will grow from a fibre break in a stable way, requiring an increasing tensile load, until it is about half-way to the edge of the specimen. This is in marked contrast to a crack in a homogeneous medium or at the horizontal interface between an elastic and a rigid material, when all cracks are, in principle, unstable.

In a fibre fragmentation test, cracking of the resin is sometimes observed, originating at the broken fibre ends [13–15]. Diameters of these resin cracks can be several hundred times larger than the fibre diameter without fracturing the specimen [13]. This feature is consistent with the observations of crack growth and crack stability reported here.

## 4.2. Effect of neighbouring fibres (Model 2)

A rigid cylindrical tube bonded to the external surface of the matrix is used here to represent neighbouring fibres surrounding a broken fibre. Calculated compliances for different values of rod radius, $R_i$, are plotted in Fig. 13 as a function of dimensionless crack radius. When the dimensionless crack radius is greater
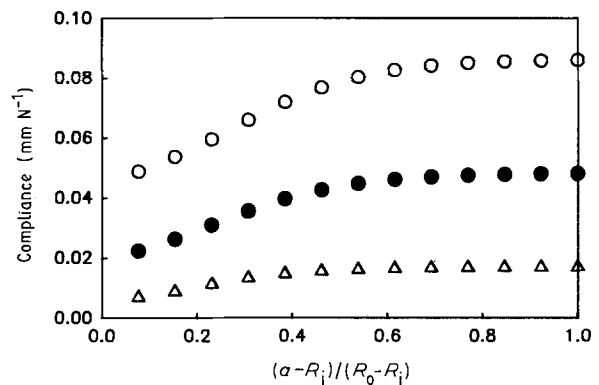


Figure 13 Compliances calculated by FEM for Model 2 specimens, with various values of rod radius $R_i$ (mm): (O) 0.435, (●) 1.00, (△) 2.00. $R_o = 3.0$ mm.

than about 0.5, the compliance is seen to reach a substantially constant value. Corresponding values of the energy release rate, $G$, obtained as before from the rate of change of compliance with crack area, are plotted in Fig. 14. They are seen to decrease over the entire range of crack radius. Thus, stable crack growth would be expected for all sizes of crack, until the crack
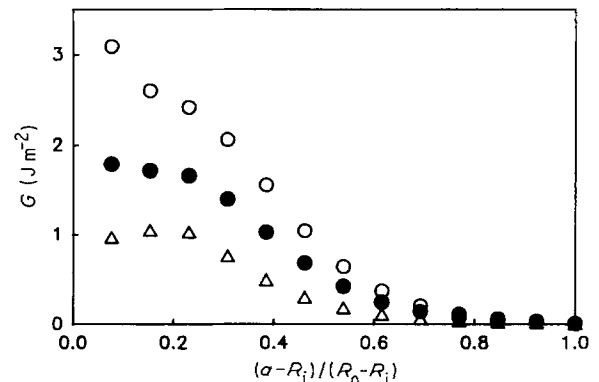


Figure 14 Calculated energy release rate, $G$, versus dimensionless crack radius for Model 2 specimens subjected to unit applied load. $R_i$ (mm): (O) 0.435, (●) 1.00, (△) 2.00; $R_o = 3.0$ mm.

reaches the surface of the externally restraining tube. Addition of the rigid tube has thus made crack growth more difficult and there is now no tendency for catastrophic growth to occur.

Force–displacement relations were determined experimentally for samples with a rigid tube bonded to the external surface of the resin. Forces due to thermal contraction were absent and, because of the external restraint, Poissonian contraction did not occur. Thus, only the effect of optical magnification needed to be taken into account in determining crack radii. The refractive index of the glass tube was assumed to be the same as that of the silicone resin.

Cracks could be observed up to a radius of 2.7 mm in a sample with resin radius of 3.0 mm, corresponding to a dimensionless crack radius of 0.9, before internal reflection prevented further viewing. Crack growth was stable up to the limit of observation. A comparison is made in Fig. 15 between the calculated relation for crack radius as a function of applied force, represented by the full curve, and experimental measurements. Good agreement is seen to obtain over the entire range of crack radius, using a value for resin fracture energy, $G_c$, of 230 J m$^{-2}$ as indicated by direct measurements on the resin.

Crack growth began at an applied force of 9.5 N, close to the value, 8.4 N, obtained by extrapolating FEM results to the initial crack size. Further crack growth required a larger force. It is clear that the presence of the external tube, representing neighbouring fibres around a broken fibre, tends to make resin cracking more difficult and prevent it from becoming catastrophic.

Thus, both the form of the crack-growth relation and the actual values of crack driving force appear to be predicted successfully for the second model, as well as for the first.

The fibre content of the composite is represented in Model 2 by the ratio of cross-sectional areas of fibre and sample, $(R_i/R_o)^2$. As this ratio was increased, the force required to propagate a crack increased, Table II.

## 5. Conclusions

In general, materials fail when the energy release rate of the system reaches a critical value, $G_c$. This criterion
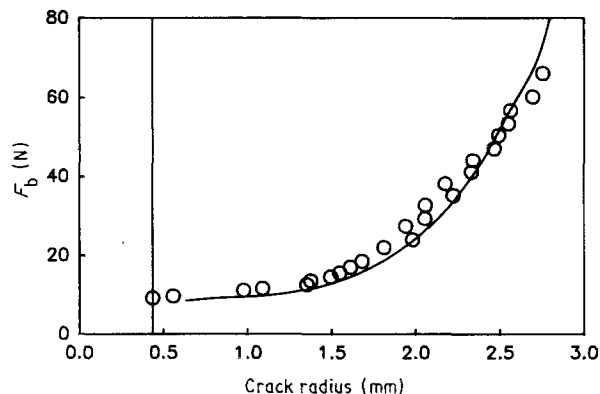


Figure 15 (——) Calculated and (○) measured values of applied load, $F$, versus crack radius for a Model 2 specimen. $R_i$ (represented by the vertical line) = 0.435 mm; $R_o$ = 3.0 mm.

TABLE II Calculated and measured forces, $F_i$, to initiate a crack in Model 2 specimens

| $R_i$ (mm) | $R_o$ (mm) | $F_i$ (N) calculated | $F_i$ (N) measured |
|---|---|---|---|
| 0.15 | 3.0 | 6.0 | |
| 1.0 | 3.0 | 11.8 | |
| 2.0 | 3.0 | 16.8 | |
| 0.435 | 2.0 | 7.5 | |
| 0.435 | 3.0 | 8.4 | 9.5 |
| 0.435 | 4.0 | 9.9 | 10.3 |

is widely used in linear elastic fracture mechanics. If $dG/dA$ is negative, an increased stress is needed to maintain crack growth. This results in stable crack growth. It has been shown that a circular crack, created by fibre fracture in a single-fibre model composite, is stable in this way until it reaches a relatively large radius, about half-way to the surface of the cylindrical resin block containing the fibre. Experimental observations are in agreement with these conclusions. The force required to propagate a crack was found to be in good agreement with values predicted by linear elastic fracture mechanics at all stages of crack growth. In particular, the maximum force that the system could support (the breaking load) was predicted successfully for a range of dimensions. On the other hand, for a model surrounded by a rigid tube representing neighbouring fibres in a closely packed fibre composite, a crack growing outwards from a broken fibre was predicted to be stable at all stages of growth, requiring an increasing force to make it grow further. Again, good agreement was found between calculated and measured values. Eventually, these specimens broke by failure of the resin in shear, after the crack tip had reached the edge of the resin cylinder. A similar analysis of this mode of failure is therefore being attempted.

## Appendix 1

Magnification of the apparent crack radius by the cylinder of resin surrounding it can be calculated as follows. As shown in Fig. A1, the angles $\theta_a$ and $\theta_b$ of light rays emerging from the cylinder can be expressed by Snell's law

$$\sin \theta_a = n \, (y_o/R_o) \tag{A1}$$

$$\sin \theta_b = n \sin [\tan^{-1} (y_o/R_o)] \tag{A2}$$

where $n$ is the refractive index of the resin ($n = 1.41$), $R_o$ is the radius of the resin cylinder, and $y_o$ is the crack radius. Equations for the light path are
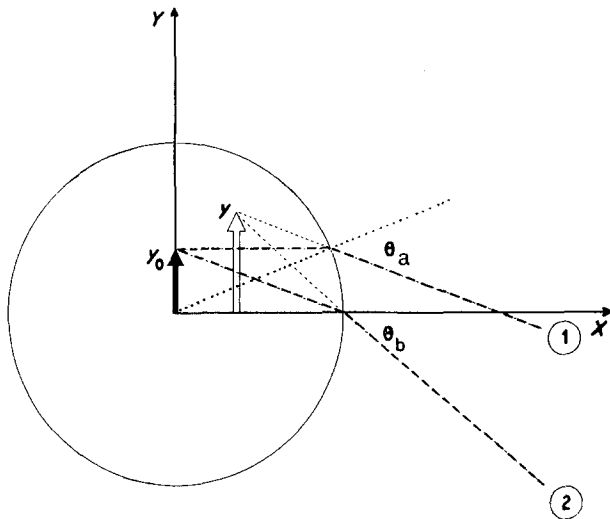
*Figure A1* Sketch of light-ray paths 1 and 2 to indicate optical magnification of crack by the resin cylinder acting as a lens.

$$y - y_o = -[x - (R_o^2 - y_o^2)]^{1/2}$$
$$\times \tan [\theta_a - \sin^{-1} (y_o/R_o)] \qquad (A3)$$

$$y = -(x - R_o) \tan \theta_b \qquad (A4)$$

The degree of magnification $y/y_o$ can be determined by inserting the actual crack size, $y_o$, into the above equations and solving for $y$. A calibration curve is given in Fig. A2, and compared with experimental measurements of the degree of magnification. Over a wide range, the magnification is about 1.4, approximately the same as the value for small angles, given by the refractive index of the resin.

Total internal reflection occurred when the incident angle was larger than a critical value. This made it impossible to measure a crack radius larger than about 70% of the cylinder radius.

## Appendix 2

When a cracked specimen is subjected to a tensile force under which the crack does not propagate but merely opens, the crack is reduced in radius by Poissonian contraction of the entire specimen. The measured crack radius is thus smaller than its actual size in the unstrained state. The higher the stress, the larger the discrepancy. An estimate of the amount of lateral contraction can be obtained by FEM, by determining the relative lateral contractile displacement of the
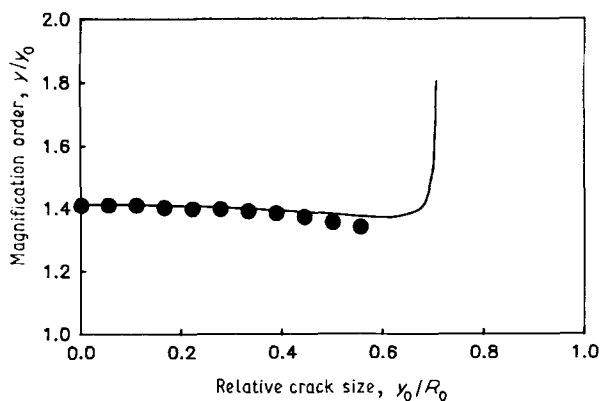


*Figure A2* Calculated magnification $y/y_o$ of the crack radius; (●) measured, (——) predicted.
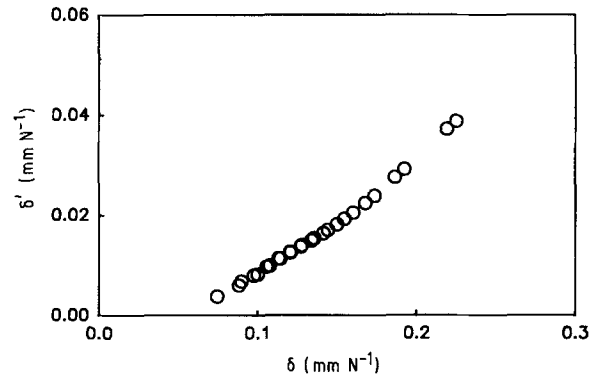


*Figure A3* Poissonian contraction of the crack radius. Lateral displacement (contraction) $\delta'$ of the crack tip versus longitudinal displacement (extension) $\delta$ of the sample, for unit applied load. $R_i = 0.435$ mm, $R_o = 3.0$ mm.

crack tip, $\delta'$, and longitudinal tensile displacement of the upper surface of the cylinder, $\delta$, for unit applied tensile load. A plot of $\delta'$ versus $\delta$ is presented in Fig. A3 for a sample with rod radius $R_i = 0.435$ mm and resin radius $R_o = 3.0$ mm. The actual crack radius is then given by

$$a_{\text{actual}} = a_{\text{observed}} + \delta' \qquad (A5)$$

## References

1. A. A. GRIFFITH, *Phil. Trans. R. Soc. (Lond)* **A221** (1920) 163.
2. A. N. GENT, G. S. FIELDING-RUSSELL, D. I. LIVINGSTON and D. W. NICHOLSON, *J. Mater. Sci.* **16** (1981) 949.
3. A. N. GENT and G. L. LIU, *ibid.* **26** (1991) 2467.
4. A. N. GENT and S. Y. KAANG, *Rubber Chem. Technol.* **62** (1989) 757.
5. A. N. GENT and O. H. YEOH, *J. Mater. Sci.* **17** (1982) 1713.
6. A. N. GENT, *Rubber Chem. Technol.* **56** (1983) 1011.
7. R. A. SACK, *Proc. Phys. Soc. (Lond.)* **58** (1946) 729.
8. V. I. MOSSAKOVSKII and M. T. RYBKA, *Prikl. Mat. Mekh.* **28** (1964) 106.
9. J. MULLIN, J. M. BERRY and A. GATTI, *J. Compos. Mater.* **2** (1968) 82.
10. J. M. MAHISHI and D. F. ADAMS, *ibid.* **16** (1982) 457.
11. *Idem., J. Mater. Sci.* **18** (1983) 447.
12. L. T. DRZAL, M. J. RICH, J. D. CAMPING and W. J. PARK, in "35th Annual Technical Conference", 1980, Reinforced Plastics and Composites Institute, Vol. 20-C, (Society of Plastics Industry, 1980) p. 1.
13. S. M. LEE and S. HOLGUIN, *J. Adhesion* **31** (1990) 91.
14. A. T. DIBENEDETTO and P. J. LEX, *Polym. Engng Sci.* **29** (1989) 543.
15. W. D. BASCOM and R. M. JENSEN, *J. Adhesion* **19** (1986) 219.
16. R. S. BARSOUM, *Int. J. Numer. Meth. Engng* **11** (1977) 85.
17. J. R. DIXON and L. P. POOK, *Nature* **224** (1969) 166.
18. J. G. WILLIAMS, "Fracture Mechanics of Polymers" (Wiley, New York, 1984) p. 30.
19. I. N. SNEDDON and M. LOWENGRUB, "Crack Problems in the Classical Theory of Elasticity" (Wiley, New York, 1970) p. 138.
20. K. J. BATHE, "ADINA: A Finite Element Program for Automatic Dynamic Incremental Non-Linear Analysis", Report no. 82448-1, Massachusetts Institute of Technology, Cambridge, MA (1977).
21. J. P. BENTHEM and W. T. KOITER, in "Methods of Analysis and Solutions of Crack Problems", edited by G. C. Sih (Noordhoff, Leyden, 1973) Ch. 3.